Full Paper
Journal of Nano Materials Impact 2026, 02 (02) 1-10

One Step and Simple Method to Synthesize Efficient Co_3O_4/NiO Electrode for Water Splitting Application

Husam A. Khamees, Osama Abdul Azeez Dakhil*
Department of Chemistry, College of Science, Mustansiriyah University, 10052 Baghdad, Iraq.

Abstract

NiO's chemical stability, high resistance to corrosion, and low cost make it a popular choice for water splitting photoanodes. The surface of nickel foil was treated with anodisation to create a nanostructured layer of nickel oxide. A Co_3O_4/NiO junction electrode was created by using an ultrasound-assisted deposition approach to evenly deposit Co nanoparticles onto NiO. X-ray diffraction was used to examine the materials' structural properties and FESEM to assess their surface shape. FE-SEM images show that the photoelectrochemical characteristics are greatly affected by the Co_3O_4 nanoparticles that are decorated on NiO. While changing the nanocomposite's overall structure, the particles' diameters are affected, with NiO having a range of 45 to 276 nm and Co_3O_4/NiO 51 to 286 nm. As the layer thickness increases, the absorption in the UV-vis range also increases. The PL study confirmed that as the layer thickness increased, the energy gap shrank from 2.98 to 2.73 eV. The NiO electrode has a photocurrent density value of 3.74 mA cm^{-2}, at the same time Co_3O_4/NiO electrode has a value of 5.99 mA cm^{-2}. While pure NiO demonstrated a conversion efficiency of 57.9% from photons to current, Co_3O_4/NiO was found to have an efficiency of 84.3%.

Keyword: nickel oxide nanostructures • water splitting • hydrogen production • anodization method • photo-electrochemical detection.

Downloaded from https://nanomatimp.uomustansiriyah.edu.iq/

Introduction

The urgent need to build alternative, clean, and renewable energy sources has been heightened by the world's reliance on fossil fuels and other politically sensitive energy sources, as well as by the unpredictable fluctuations in the price of crude oil[1]. In order to meet the increasing global need for energy, scientists have been exploring environmentally friendly, cost-effective, and straightforward methods of generating renewable energy[2]. When compared to traditional fossil fuels, solar power is both more inexpensive and more environmentally friendly. Among the several solar energy conversion methods, photoelectrochemical (PEC) water-splitting stands out as an essential and sustainable answer to the global energy crisis. Quickly, it separates oxygen and hydrogen from water by utilising sunlight and semiconducting PEC materials[3]. PEC water-splitting, or PEC, is a crucial and long-term method for converting solar energy. It quickly separates hydrogen and oxygen from water molecules by using sun radiation and semiconducting PEC materials[3]. In 1972, Fujishima and Honda became the first to study photocatalytic water splitting when they discovered that a semiconductor TiO_2 electrode could produce hydrogen when exposed to ultraviolet light [4].

Methods such as heterojunctions/homojunctions[5-7], molecular design[8-12], surface loading of cocatalysts[13, 14], and heteroatom doping[15] have been developed to successfully separate electron-hole pairs and limit charge recombination. Loading semiconductor photocatalysts with cocatalysts is one approach of enhancing their photocatalytic activity. So, the photocatalysts are more stable, the photogenerated charges are better separated, more active sites are exposed, and they are better able to capture light. Cocatalysts are thus a powerful tool for improving photocatalytic H_2 evolution[16, 17].

Nanoscience is a hot topic in the scientific community, although most discussions, definitions, and focus are on nanotechnology. So, it's a general term that describes how much people like learning about topics that could be useful to them in the actual world[18]. Nanotechnology combines the most basic aspects of the biological, physical, and chemical sciences. These processes occur at the nanoscale. Reducing size is one thing, whereas controlling chemical properties and creating new chemical connections is another[19, 20].

Since nanotechnology controls materials on a scale one billion times smaller than a metre, it is technologically innovative.

Since nanotechnology controls materials on a scale one billion times smaller than a metre, it is technologically innovative. Actually, nanotechnology encompasses all technologies that work on the nanoscale and have several real-world applications[21].

***Address for correspondence:** Prof. Dr. Osama Abdul Azeez Dakhil, Department of Chemistry, College of Science, Mustansiriyah University, 10052 Baghdad, Iraq.
E-mail: dr.osama@uomustansiriyah.edu.iq
ORCID: https://orcid.org/0000-0002-6099-7311

This is an open-access journal, and articles are distributed under the terms of the Creative Commons Attribution License (CC-BY) 4.0 License, which allows others to use, distribute, and reproduce in any medium for noncommercial purposes, as long as the original work is cited properly.

Info:
Submitted: 3 May 2026; **Revised:** 20 June 2026;
Accepted: 11 July 2026; **Published:** 15 Aug. 2026.
https://doi.org/10.71109/nmi.2026.2.2.29

Copyright © 2026. This work licensed under a Creative Commons Attribution Noncommercial 4.0 International License.

Electrospinning, hydrothermal synthesis, vapour deposition, precipitation from micromulsions, mechanochemical processes, and precipitation are some of the ways that NiO particles of different sizes, shapes, and spatial configurations can be produced. Using these methodologies to adjust reaction conditions allows for the customisation of nickel oxide nanoparticle synthesis for different applications[22]. As a p-type semiconductor, NiO has a band gap energy between 3.5 and 4.0 eV[23].

Hydrothermal, wet chemical, sol-gel, electro-deposition, and anodisation procedures are among those described for the manufacture of porous oxide materials. Because it is easy and effective to use, anodisation has attracted a lot of attention for creating porous structures on many metals [24]. Anodisation, or electrochemical oxidation, is a process that can produce oxide layers with different metal surfaces [24]. Reason being: it's economical, friendly to the environment, and easy to use[25].

This research aims to evaluate the structural properties of NiO and Co_3O_4/NiO through their simple and cost-effective production. The next step is to split water using PEC technology in order to create hydrogen (H_2).

Experimental and Methods

Preparation of NiO

Before using an air stream to dry it, it was rinsed with DI water. Next, sonicate the Ni foil in 100% acetone for 10 minutes to clean and polish it for this task. Pieces of 0.25 mm thick, 99.8% pure nickel foils were sliced into 1.2 × 1.2 cm^2 pieces, and then NiO was created using the electrochemical anodisation technique. The process of anodising was carried out at ambient temperature. The anodisation procedure was carried out using a handmade cylindrical Teflon cell. A Ni foil working electrode and a (25 × 25 × 3) mm^3 graphite plate counter electrode are both included in the cell. In 100 mL of deionised water (H_2O), 11.222 g of 97.9% pure KOH (2 M) was dissolved to create the electrolyte solution. The distance between the electrodes was kept constant at 2.3 cm throughout all experiments. Presented here is the process of electrochemical anodisation: The first step was to apply a 2.5 V voltage to the electrodes for 60 minutes. Secondly, the nanostructures were rinsed with DI and then air-dried following preparation. The next process was annealing the nanostructures in a box furnace, where the temperature was raised from ambient temperature to 350 °C 10 °C each minute. We kept the temperature at that level for an hour. The next step was to let the sample cool down naturally within the furnace.

Decorating of NiO by COBALT (Co)

For 30 minutes, NiO was irradiated in a 0.05M [Co $(NO_3)_2 \cdot 6H_2O$] aqueous solution using an ultrasonic generator (VGT-1730 QT) running at 40 kHz and 100W. Decorated NiO containing Co NPs was achieved at room temperature via assisted deposition. After the Co deposition, the samples were rinsed in DI to remove any excess NiO ions, and then dried with hot air. To enhance the crystallinity of the structure and debond the $CO(NO_3)_2$ molecules, the as-prepared samples were subjected to atmospheric heating at 350 °C for 60 minutes at a rate of 10 °C/min to obtain NiO/Co_3O_4. **Figure 1** depicts the experimental setup for the manufacture of NiO from nickel foils, and the decorating process of Co_3O_4 is schematically indicated. The disintegrating Co, O, and N atoms were later changed into Co_3O_4 NPs and NO↑/O_2↑.

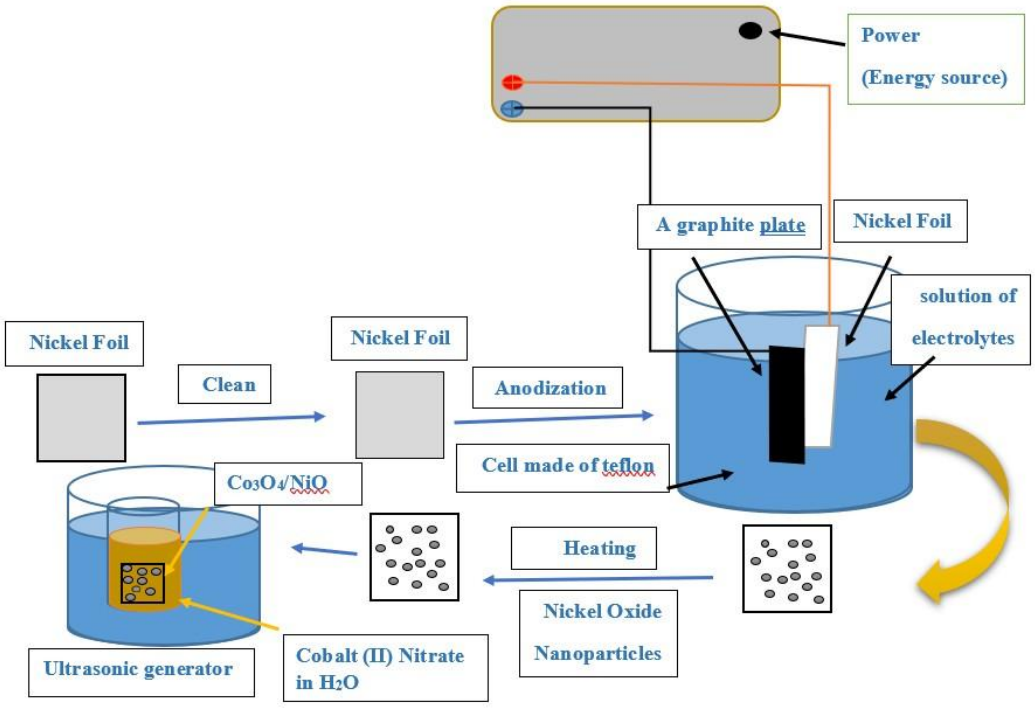


Figure 1. Steps of the anodization process and preparation of Co_3O_4/ NiO.

Downloaded from https://nanomatimp.uomustansiriyah.edu.iq/

Copyright © 2026. This work licensed under a Creative Commons Attribution Noncommercial 4.0 International License.

Characterization

Miniflex II Rigaku of Japan experimented using X-ray diffraction and a CuKα source with a wavelength of 1.5408 Å. To find out what the elements were, scientists employed powerful X-ray spectroscopy. A field-emission scanning electron microscope TESCAN MIRA3 is used to study the surface morphology of NiO and Co_3O_4 NPs. The PL spectra were measured using a Shimadzu spectrofluorophotometer of the RF-5301PC type, which excites the sample at 300 nm using a xenon lamp.

Photoelectrochemical Measurements

The PEC measurements were carried out in an electrolyte solution containing 0.4 M NaOH. The working electrodes (WE) were made of different samples of Co_3O_4/NiO, the reference electrodes (RE) were constructed of Ag/AgCl, and the counter electrodes (CE) were a graphite sheet. The cell's source is a 4 × 2 cm^2 quartz window that allows light to pass through. The reference electrode for all potential measurements in this work was a 55 W Xenon light source with an Ag/AgCl composition. The solar simulator achieved a power density of 20 mW/cm^2. The samples were exposed to radiation at a certain wavelength using a monochromator.

J-V characteristics of the current density with respect to the applied potential were quantified using the Keithley-2430 source meter unit. At a bias voltage of 0.8 V relative to Ag/AgCl, the spectral response was observed, which varied with wavelength. The Electrochemical Cell experimental setup is illustrated schematically in **Figure 2**.

The photon-to-current conversion efficiencies (IPCE) efficiency of pure NiO and Co_3O_4/NiO was determined using the following equation[26]**:**

$$IPCE\ (\%) = \frac{1240\ \times Jph\ \left(\frac{mA}{cm^2}\right)}{\lambda\ (nm) \times Iinc\ \left(\frac{mW}{cm^2}\right)} \times 100\% \quad \text{... (1)}$$

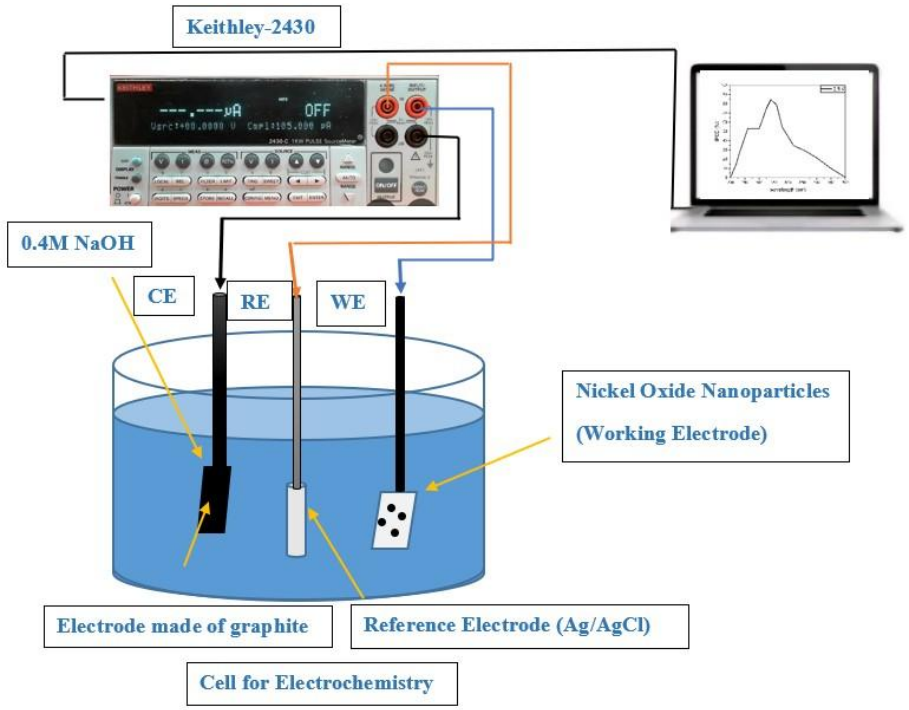


Figure 2. Setup of PEC cell measurements.

Results and Discussion

Structural Analysis (XRD)

Electrochemical anodisation of NiO and Co_3O_4/NiO yielded data that can be utilised to understand their structural properties; these are shown in **Figure 3**. Two peaks at 2θ values of 44.47° and 76.39°, which correspond to (2 0 0) and (3 1 1), respectively, may be seen in the XRD patterns of NiO. Everything about these diffraction peaks is in agreement with the conventional diffraction data, according to the XRD patterns (JCPDS 47–1049)[27]. The X-ray diffraction investigation confirmed this complete transition to NiO. The average crystallite size t_{hkl} has been calculated using the Debye-Scherer formula as given by the following equation[28].

$$t_{hkl} = \frac{0.98\lambda}{\beta Cos\theta} \quad \text{... (2)}$$

where λ is the wavelength of the X-Ray radiation and β is the full width at half maximum (FWHM) at diffraction angle θ. NiO crystallites typically measure 17.43 nm in size.

According to the XRD patterns (JCPDS 47-1049)[29], the 2θ values of 44.57° and 76.51°, which represent the reflection planes of (2 0 0) and (3 1 1), respectively, are in good agreement with the standard diffraction data for Co_3O_4/NiO. The patterns observed here demonstrate that the decoration of NiO with Co_3O_4 NPs had no effect on the phase structure of the material. The low concentration and uniform dispersion

Downloaded from https://nanomatimp.uomustansiriyah.edu.iq/

Copyright © 2026. This work licensed under a Creative Commons Attribution Noncommercial 4.0 International License.

of Co_3O_4 NPs on NiO could be the reason behind this[30, 31]. Crystallites of Co_3O_4/NiO typically measure 105.26 nm in size.

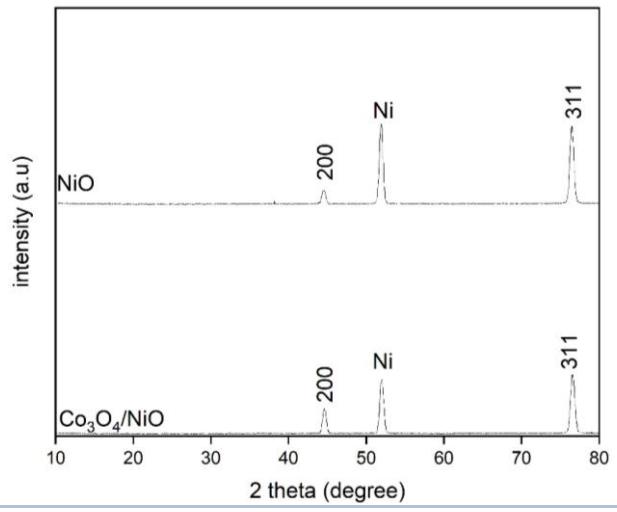


Figure 3. XRD spectra of NiO and Co_3O_4/ NiO.

The FESEM Images of IONPs

The FESEM study of the NiO sample revealed a uniformly shaped and sized particle distribution and an approximately spherical particle shape. The samples displayed in Figure 4 typically contain NiO nanoparticles ranging in size from 45 to 276 nm. **Figure 4** shows the size distribution histogram of the synthesised NiO nanoparticles, which were created by the Image J software using the spherical particle size assumption (as shown in **Figure 5**).

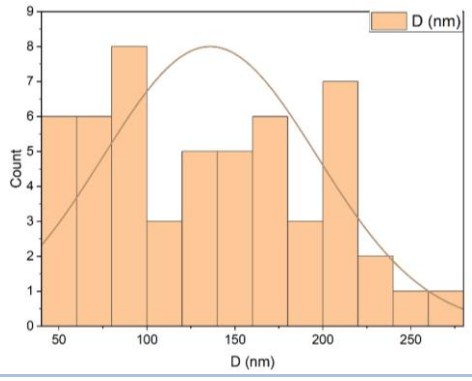


Figure 4. Size distribution histogram of NiO nanoparticles.

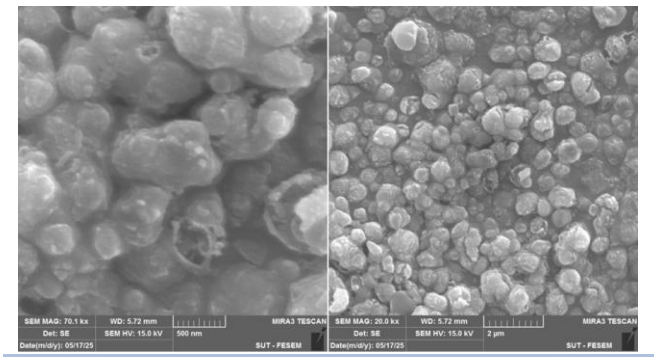


Figure 5. FESEM images of the NiO electrode anodized at 2.5V.

Within a wide range centred on the main value, particles in this picture have a diameter of about 136 nm. Figure 5 shows the result of fitting this modal distribution with a Gaussian function; the resulting mean particle diameter is d = 136 nm.

Particles in the Co_3O_4/NiO sample are uniformly dispersed and have a fiber-like structure, according to FESEM research. **Figure 6** shows that the samples included Co_3O_4/NiO nanoparticles with an average size of (51-286) nm. The size distribution histogram of the synthesised Co_3O_4/NiO nanoparticles (**Figure 7**) was created by the Image J software, based on the spherical particle size assumption (**Figure 6**). The image shows particles with a diameter of about 146 nm, which falls somewhere in the center of a wide distribution around the main value. Figure 7 shows the result of fitting this model distribution with a Gaussian function; the result is the mean particle diameter, d = 146 nm.

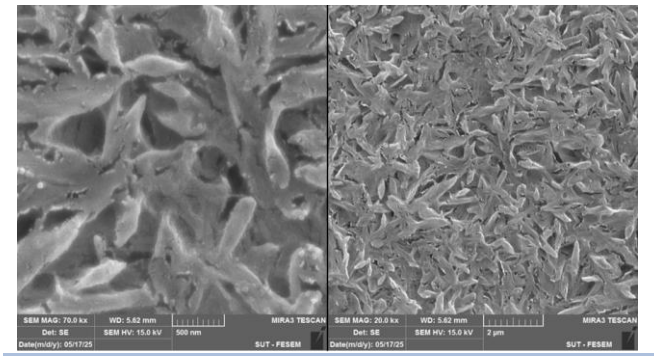


Figure 6. FESEM pictures of the Co_3O_4/NiO electrode anodized at 2.5 V.

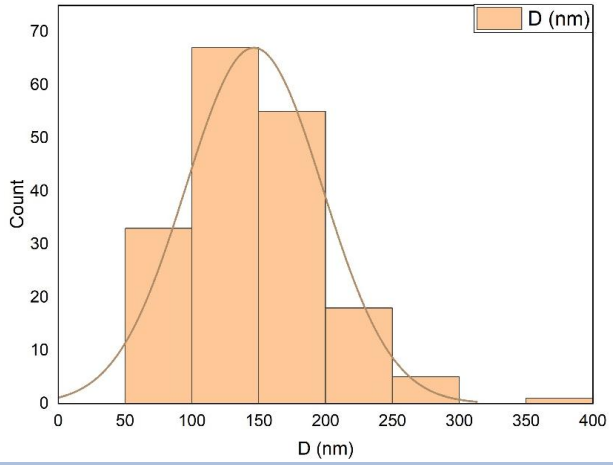


Figure 7. Size distribution histogram of Co_3O_4/NiO nanoparticles.

EDX of NiO and Co3O4/NiO Heterojunctions

Figure 8 shows the EDX spectra of NiO nanoparticles that were either coated with 0.05 M Co concentrations or were generated at 2.5 V through anodisation. On this page you may see the samples' chemical make-ups. It is clear from the patterns that Ni, O, and Co are the main elements in the sample. The samples contained contaminants such as Na, S, Cl, K. Tables 1 and Tables 2 show the elemental compositions of the NiO and Co_3O_4/NiO electrodes, respectively.

Downloaded from https://nanomatimp.uomustansiriyah.edu.iq/

Copyright © 2026. This work licensed under a Creative Commons Attribution Noncommercial 4.0 International License.

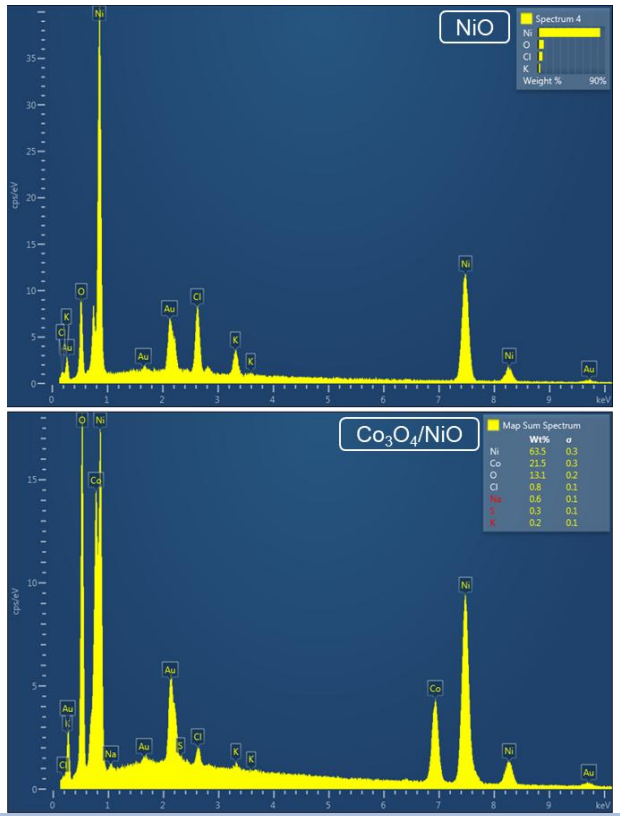


Figure 8. The EDS spectrum of the NiO and Co_3O_4/ NiO electrode.

Photoluminescence Spectra

Figure 9 shows the photoluminescence (PL) emission spectrum. At 455 nm, or 2.73 electron volts, the Co_3O_4/NiO exhibits its strongest emission peak. However, it was discovered that the UV strong emission peak for NiO was 415 nm, or 2.98 eV, when stimulated at 319 nm. The intrinsic transition of the excitons from the conduction band to the valence band causes this type of emission and the accompanying peak, which are triggered by Ni^{2+} ion transitions involving $3d^8$ electrons[32]. Furthermore, the final emission spectrum shows emission maxima at around 574 nm. Possible sources of the extra emission peaks at 350 °C annealing temperature include oxygen-related flaws or near-band-to-band transitions[33]. The presence of cation vacancies or interstitial oxygen trapping in the NiO lattice is confirmed by the prominent emission peak at 667 nm. Heat treatment can produce a slight divergence from NiO stoichiometry, according to other sources[34].

Although Co_3O_4/NiO does not add any emission when compared to undecorated NiO, it drastically changes the PL intensity. The PL intensity of the painted sample is higher than that of pure NiO. According to the EDX findings, the presence of additional surface oxygen vacancies and flaws can increase the PL intensity of the decorated samples. Photoluminescence (PL) emission is made possible by the easy binding of photo-induced electrons to excitons at certain oxygen vacancy and bandgap defect levels[35].

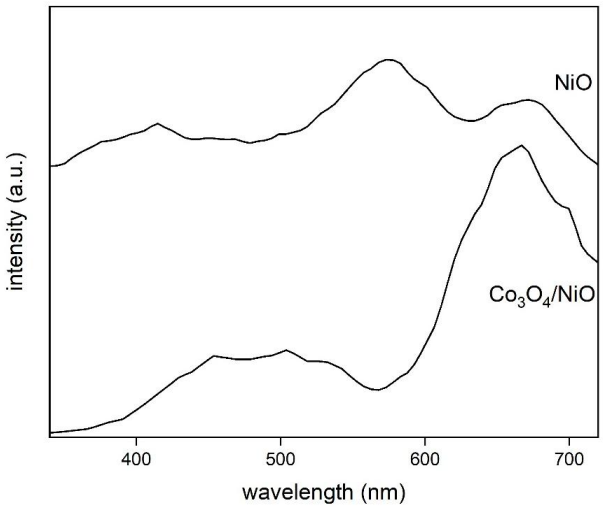


Figure 9. PL spectra of the NiO and Co_3O_4/ NiO electrodes.

Photoelectrochemical Performance of NiO and Co_3O_4/NiO

In order to explore the PEC activities of pure NiO and Co_3O_4/NiO nanoparticles, the J-V characteristics were determined in a three-electrode cell. The cell was designed with a graphite plate as the counter electrode and Ag/AgCl as the reference electrode. The reference electrode for all potential measurements in this work was a 55 W Xenon light source with an Ag/AgCl composition. The solar simulator achieved a power density of 20 mW/cm^2. The samples were exposed to radiation at a certain wavelength using a monochromator. At 0.8 V vs Ag/AgCl, the J-V characteristics were measured in a 0.4 M NaOH solution, as shown in **Figure 10**.

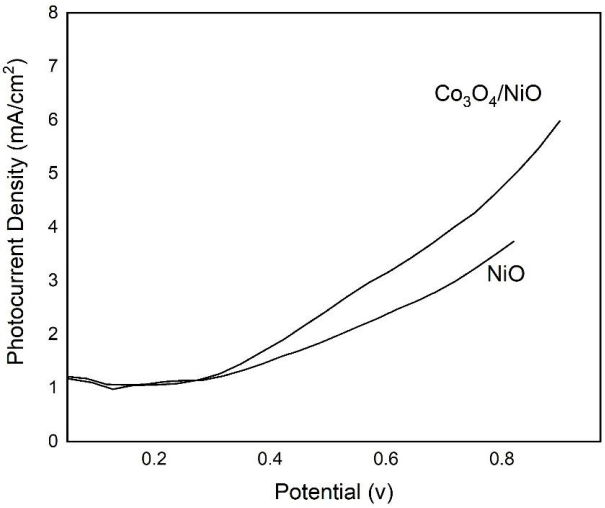


Figure 10. J–V characteristics of the pure NiO and Co_3O_4/ NiO illuminated electrodes.

Under the same conditions, the pure NiO As electrode shows a photocurrent density of about 3.74 mA cm^{-2}, whereas the Co_3O_4/NiO electrode combination showed better results, displaying an improved photocurrent density of around 5.99 mA cm^{-2}.

Downloaded from https://nanomatimp.uomustansiriyah.edu.iq/

Copyright © 2026. This work licensed under a Creative Commons Attribution Noncommercial 4.0 International License.

Downloaded from https://nanomatimp.uomustansiriyah.edu.iq/

According to our research, adding Co_3O_4 to HER catalysts increased their catalytic activity. That makes sense, considering that decorating with Co_3O_4 would increase the intrinsic activity of each active site[36]**.** If oxygen faults do occur, then all electrocatalysts should have a good OER reaction, according to PL research[37]**.** Electrochemical reactions involve the oxidation of Ni^{2+} ions on NiO electrode surfaces to Ni^{3+} ions. The ensuing oxygen evolution events are aided by these ions as they facilitate the oxidative reaction of water[37, 38].

According to PL spectroscopy, the greater photocurrent density of Co_3O_4/NiO is explained by its enhanced visible light PEC activity. This is because electron-hole couples are effectively separated. These results support the idea of a photocatalytic method for producing hydrogen using Co_3O_4/NiO sheets as photoelectrodes. Initially, in a light-activated NiO thin film, a hole (h^+) is created in the valence band when an energy-absorbing electron (e^-) transfers from the valence band to the conduction band. A pair of holes and electrons are created as a result, and they eventually make their way to the surface[39]. Electrons are quite fragile when they enthusiastically enter the conduction band. Reaching the valence band again, they re-join the gap. Quantum yield in the photocatalytic reaction is consequently reduced. A reduction in the charge carrier recombination rate using Co_3O_4 can improve the photocatalytic efficiency. Their ability to prolong the lifetime of electrons makes them an ideal charge trap for photogenerated carriers. The electronic states of the Co atoms trap the charge carrier[40]. The photocatalytic effectiveness is improved by lowering the chance of recombination, which allows trapped charges to be transported to the surface of the film for reaction. This surface is dominant due to its rapid surface mobility and the recombination of charge carriers generated by photocatalysis [41]. Furthermore, the thin film exhibited improved photocatalytic activity as a result of the increased surface affinity of the adsorbed water caused by the Co-induced defects in NiO[42, 43].

Figure 11 displays the photocurrent density spectra obtained in the 360-600 nm range for both pure NiO and Co_3O_4/NiO electrodes. Optimal surfaces for adsorbing oxygen-related compounds, high conductivity, a large number of active sites, and low oxygen vacancies make the composite catalyst an attractive choice for water splitting. The suggested mechanism for water splitting could be explained by the synergistic action of NiO and Co_3O_4/NiO nanocomposite, which improves water dissociation and may alter the electronic structure to reduce hydrogen adsorption. This could result in an ideal zone. Therefore, the catalyst showed remarkable bifunctional performance in water splitting, displaying both oxygen evolution reaction (OER) and hydrogen evolution reaction (HER) properties in a single alkaline electrolyte. Surface property adjustment, which could improve water splitting performance, could also be achieved by depositing cobalt oxide on top of NiO nanostructures. It is possible that pure NiO and Co_3O_4 will not work due to their poor conductivity and lack of activity toward water dissociation. Nanocomposites made of the two materials, on the other hand, could improve water splitting thanks to their surface-tailored properties and abundance of active sites. Increased water dissociation results from the nanocomposite's synergistic effects and high conductivity, as evidenced by the HER and OER polarisation curves at low potentials[44].

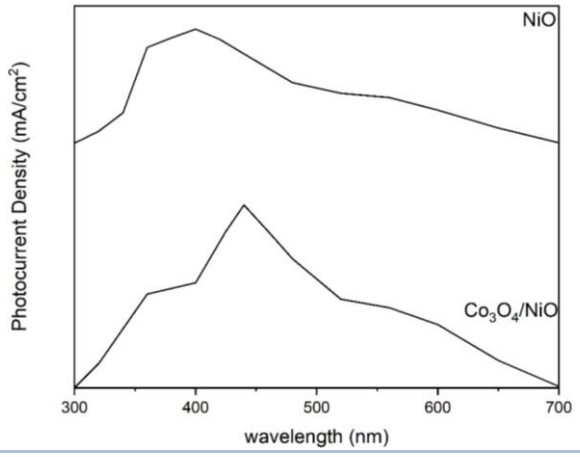


Figure 11. The photocurrent response vise wave length of the NiO electrode and the Co_3O_4 NPs decorated NiO electrode.

The photocurrent densities of NiO and Co_3O_4 electrodes peak at approximately 400 nm and 440 nm, respectively. Comparing the photocurrent density of the NiO electrode with and without decorated Co_3O_4 reveals an improvement in the 400-440 nm range. No longer were the photocurrent densities of NiO and Co_3O_4/NiO electrodes the same (**Figure 12**).

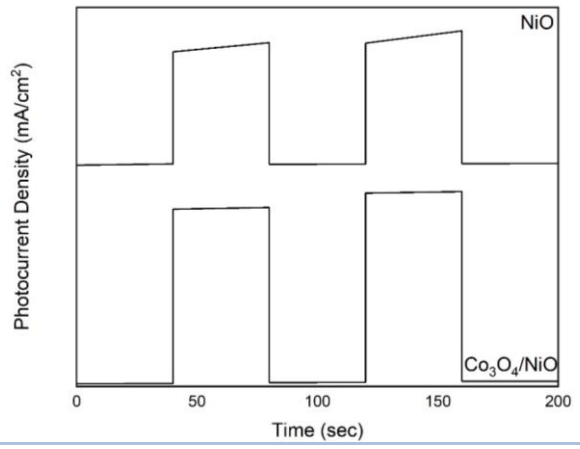


Figure 12. The photocurrent density response of NiO, with and without decorating Co_3O_4.

A wide range of wavelengths, from 360 to 600 nm, were used to test each of the manufactured electrodes. With a bias voltage of 0.8 V in a 0.4 M NaOH solution, the maximum photocurrent response at 440 nm was 40 s of off-and-on time. The two electrodes exhibit almost no photocurrent response even when subjected to light, hence disproving the existence of any electrocatalytic action. Various wavelengths of irradiation were used to examine the samples' incident IPCEs at an applied voltage of 0.8 V. According to the findings, the quantum efficiency of the Co_3O_4/NiO electrode is higher than that of the pure NiO electrode in the UV-Vis spectrum.

Copyright © 2026. This work licensed under a Creative Commons Attribution Noncommercial 4.0 International License.

Based on the results from **Figure 11** and Equation 1, the IPCE spectra for pure NiO and Co_3O_4/NiO, as a function of excitation wavelength, are displayed in Fig. 14. The separation efficiency of electron-hole (e^-/h^+) pairs is a well-known determinant of the photoelectrochemical efficiency. As may be seen in **Figure 12**, the Co_3O_4/NiO electrode's IPCE spectra exhibit a great deal.

At different excitation wavelengths (λ), the photocurrent density (J_{ph}) and incident light intensity (Iinc) are measured. The IPCE spectra for pure NiO and Co_3O_4/NiO, as a function of excitation wavelength, are shown in **Figure 13**, based on the results from **Figure 11** and Equation 1. It is widely recognised that the photoelectrochemical efficiency is determined by the separation efficiency of e^-/h^+ couples. **Figure 12** shows the IPCE spectra of the Co_3O_4/NiO and NiO electrodes, which show a lot.

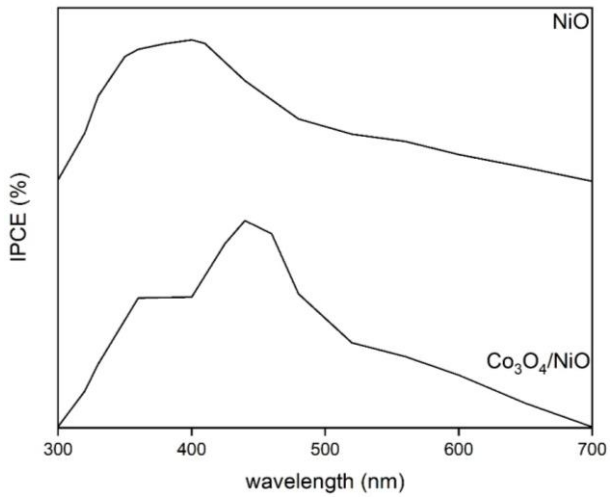


Figure 13. IPCE of the pure NiO and Co_3O_4/ NiO electrodes.

Performs better than the pure NiO electrode. The IPCE of the Co_3O_4/NiO electrode is 84.3% at 440 nm, which is significantly more than the IPCE of the pure NiO electrode, which is 57.9%. Some acceptable explanations are as follows. Because its photocurrent response spectra are redshifted relative to those of the pure NiO electrode, the Co_3O_4/NiO electrode is able to absorb both ultraviolet and visible light after it has passed through the NiO NPs.

A photoanode's photo-carrier transmission and photo-conversion efficiency can be enhanced by coupling two or more kinds of semiconductor materials. It is possible that the creation of heterostructures is responsible for the improvement of composites' PEC capability[45].

Its use in PEC water splitting is limited by NiO's slow kinetics of water oxidation and low efficiency of charge separation. The results show that the photoelectrode's outstanding PEC water splitting performance was caused by the Co_3O_4/NiO, which improved charge transfer and accelerated the kinetics of the water oxidation reaction [46].

When the hydrogen evolution and oxygen evolution reactions were driven by visible light, the catalytic activity and charge transport characteristics of NiO were enhanced by decorating it with Co_3O_4. By increasing the range of visible light that could be absorbed, this heterojunction facilitated charge separation by decreasing the recombination of photogenerated electron-hole pairs.

Heterojunction formation between NiO and Co_3O_4 improves photocatalytic efficiency. The integration causes an increase in the density of energy states, which in turn decreases the energy band gap of pure NiO by reducing its recombination rate. Additionally, the optical absorption spectra shifted favourably toward longer wavelengths as a result of this alteration, which facilitated electron transitions. Because of its better optical absorption qualities, the composite catalyst showed more promise for visible light.

The band gap of the NiO electrode is 2.98 eV, as shown in Figure 10. At the same time, the band gap for Co_3O_4/NiO is 2.73 eV. A wider absorption spectrum is the consequence of a considerable improvement in optical absorption, as the band gap narrows from 2.98 to 2.73 eV. An increase in photocatalytic efficiency was a byproduct of this broadening of the absorption spectra, which boosted electron-hole pair formation.

Figure 4 displays NiO particles with an approximately spherical shape, with variation in size and a fairly homogeneous distribution of particles. Figure 6 confirms a fiber-shaped structure of Co_3O_4/NiO. By forming an intimate and direct contact with NiO's surface, these Co_3O_4/NiO particles encase NiO. caused a unique heterostructure to develop, which improved the practicality of visible light-driven photocatalytic activity by decreasing the electron-hole recombination rate [47].

Conclusion

Finally, the Co_3O_4/NiO As connection is an attractive, sustainable, and environmentally friendly option for water-splitting applications since it can be built using a cost-effective and practical approach. This work demonstrates the synthesis of NiO nanostructures and Co_3O_4/NiO heterojunctions. Aligned rods are produced by uniformly coating NiO with Co_3O_4 using an easy ultrasonication technique. The anodisation procedure was carried out using a cylindrical Teflon cell that was manufactured. The cell's working electrode is Ni foil, while the counter electrode is a graphite plate. A PEC cell was used to study the photoelectrochemical properties of NiO and Co_3O_4/NiO, with a cheap graphite plate serving as the counter electrode. The findings reveal that the Co_3O_4/NiO electrode outperformed the others in terms of photo current and surface quality. Additionally, the Co_3O_4/NiO junction electrode showed a notable increase in photoelectrochemical activity in the presence of visible light. A larger surface area and an improvement in electron transfer efficiency are two potential causes of these results. These findings suggest that Co_3O_4/NiO might be a useful photoanode for water splitting.

Acknowledgment

The authors acknowledge the Department of Physics, College of Science, Mustansiriyah University, Baghdad, Iraq, for their support of this project.

Downloaded from https://nanomatimp.uomustansiriyah.edu.iq/

Copyright © 2026. This work licensed under a Creative Commons Attribution Noncommercial 4.0 International License.

Statement on Data Availability

All data, including any supplementary files, supporting the study's conclusions, are incorporated within the paper.

Declaration of Competing Interests

The authors assert that none of the work in this publication was affected by any recognised financial conflicts or personal relationships.

Funding

All authors declare the absence of any financial or non-financial interests or funding.

Author contribution

Husam A. Khamees conducted the experimental research and accompanying graphics for this subject. Drafting the manuscript, interpreting results, and doing the final review by Osama, AA.D. Both authors conducted the preliminary drafting of the manuscript.

References

[1] Z. Shao, T. Zeng, Y. He, D. Zhang, and X. Pu, "A novel magnetically separable $CoFe_2O_4/Cd_{0.9}Zn_{0.1}S$ photocatalyst with remarkably enhanced H_2 evolution activity under visible light irradiation," *Chemical Engineering Journal*, vol. 359, p. 485–495, 2019.

https://doi.org/10.1016/j.cej.2018.11.163.

[2] R. S. Kammel and R. S. Sabry, "Effects of the aspect ratio of ZnO nanorods on the performance of piezoelectric nanogenerators," *Advanced Materials*

Devices, vol. 4, no. 3, p. 420–424, 2019.

https://doi.org/10.1016/j.jsamd.2019.08.002.

[3] R. A. S. A. Alkareem, B. M. Ahmed, and O. A. A. Dakhil, "CuO/Cu Nanoparticles via Non-thermal Atmospheric Plasma for Photoelectrochemical Water-Splitting Application," *Journal of Electronic Materials*, vol. 53, no. 6, p. 3358–3367, 2024.

https://doi.org/10.1007/s11664-024-11022-y.

[4] A. Fujishima and K. Honda, "Electrochemical photolysis of water at a semiconductor electrode," *Nature*, vol. 238, no. 5358, p. 37–38, 1972.

https://doi.org/10.1038/238037a0.

[5] X. Yang *et al.*, "Facile fabrication of acidified g-C3N4/g-C3N4 hybrids with enhanced photocatalysis performance under visible light irradiation," *Applied Catalysis B: Environmental*, vol. 193, p. 22–35, 2016.

https://doi.org/10.1016/j.apcatb.2016.03.060.

[6] C. Ji, S.-N. Yin, S. Sun, and S. Yang, "An in situ mediator-free route to fabricate Cu2O/g-C3N4 type-II heterojunctions for enhanced visible-light photocatalytic H2 generation," *Applied Surface Science*, vol. 434, p. 1224–1231, 2018.

https://doi.org/10.1016/j.apsusc.2017.11.233.

[7] G. Liu *et al.*, "In situ bond modulation of graphitic carbon nitride to construct p–n homojunctions for enhanced photocatalytic hydrogen production," *Advanced Functional Materials*, vol. 26, no. 37, p. 6822–6829, 2016.

https://doi.org/10.1002/adfm.201602779.

[8] W. Wang, G. Li, T. An, D. K. Chan, J. C. Yu, and P. K. Wong, "Photocatalytic hydrogen evolution and bacterial inactivation utilizing sonochemical-synthesized g-C3N4/red phosphorus hybrid nanosheets as a wide-spectral-responsive photocatalyst: the role of type I band alignment," *Applied Catalysis B: Environmental*, vol. 238, p. 126–135, 2018.

https://doi.org/10.1016/j.apcatb.2018.07.004.

[9] L. Kong *et al.*, "Site-selected N vacancy of g-C3N4 for photocatalysis and physical mechanism," *Applied Materials Today*, vol. 13, p. 329–338, 2018.

https://doi.org/10.1016/j.apmt.2018.10.003.

[10] J. Cao, W. Nie, L. Huang, Y. Ding, K. Lv, and H. Tang, "Photocatalytic activation of sulfite by nitrogen vacancy modified graphitic carbon nitride for efficient degradation of carbamazepine," *Applied Catalysis B: Environmental*, vol. 241, p. 18–27, 2019.

https://doi.org/10.1016/j.apcatb.2018.09.007.

[11] F. Du, Q.-Y. Chen, and Y.-H. Wang, "Effect of annealing process on the heterostructure CuO/Cu_2O as a highly efficient photocathode for photoelectrochemical water reduction," *Journal of Physics Chemistry of Solids*, vol. 104, p. 139–144, 2017.

https://doi.org/10.1016/j.jpcs.2016.12.029.

[12] J.-W. Zhang, S. Gong, N. Mahmood, L. Pan, X. Zhang, and J.-J. Zou, "Oxygen-doped nanoporous carbon nitride via water-based homogeneous supramolecular assembly for photocatalytic hydrogen evolution," *Applied Catalysis B: Environmental*, vol. 221, p. 9–16, 2018.

https://doi.org/10.1016/j.apcatb.2017.09.003.

[13] J. Li, G. Zhan, Y. Yu, and L. Zhang, "Superior visible light hydrogen evolution of Janus bilayer junctions via atomic-level charge flow steering," *Nature communications*, vol. 7, no. 1, p. 11480, 2016.

https://doi.org/10.1038/ncomms11480.

[14] L. Zhu, Q. Yue, D. Jiang, H. Chen, R. M. Irfan, and P. Du, "Metal-free graphene quantum dots photosensitizer coupled with nickel phosphide cocatalyst for enhanced photocatalytic hydrogen production in water under visible light," *Chinese Journal of Catalysis*, vol. 39, no. 11, p. 1753–1761, 2018.

https://doi.org/10.1016/S1872-2067(18)63135-3.

[15] S. Guo *et al.*, "P-doped tubular g-C3N4 with surface carbon defects: universal synthesis and enhanced visible-light photocatalytic hydrogen production," *Applied Catalysis B: Environmental*, vol. 218, p. 664–671, 2017.

https://doi.org/10.1016/j.apcatb.2017.07.022.

Downloaded from https://nanomatimp.uomustansiriyah.edu.iq/

Copyright © 2026. This work licensed under a Creative Commons Attribution Noncommercial 4.0 International License.

[16] X. Yang, J. Xu, T. Wong, Q. Yang, and C.-S. Lee, "Synthesis of In_2O_3–In_2S_3 core–shell nanorods with inverted type-I structure for photocatalytic H_2 generation," *Physical Chemistry Chemical Physics*, vol. 15, no. 30, p. 12688–12693, 2013.

https://doi.org/10.1039/c3cp51722e.

[17] L. Huang, X. Wang, J. Yang, G. Liu, J. Han, and C. Li, "Dual cocatalysts loaded type I CdS/ZnS core/shell nanocrystals as effective and stable photocatalysts for H_2 evolution," *The Journal of Physical Chemistry C*, vol. 117, no. 22, p. 11584–11591, 2013.

https://doi.org/10.1021/jp400010z.

[18] M. Nasrollahzadeh, S. M. Sajadi, M. Sajjadi, and Z. Issaabadi, "An introduction to nanotechnology," in *Interface Science and Technology*, vol. 28: Elsevier, 2019, pp. 1–27.

https://doi.org/10.1016/B978-0-12-813586-0.00001-8.

[19] S. Malik, K. Muhammad, and Y. Waheed, "Nanotechnology: a revolution in modern industry," *Molecules*, vol. 28, no. 2, p. 661, 2023.

https://doi.org/10.3390/molecules28020661.

[20] B. Bhushan, "Introduction to Nanotechnology," in *Springer Handbook of Nanotechnology*: Springer, 2007, pp. 1–12.

https://doi.org/10.1007/978-3-540-29857-1_1.

[21] R. Sharma, K. S. Sharma, and D. Kumar, "Introduction to Nanotechnology," in *Nanomaterials in Clinical Therapeutics*, 2022, pp. 1–31.

https://doi.org/10.1002/9781119857747.ch1.

[22] S. D. Dhas *et al.*, "Synthesis of NiO nanoparticles for supercapacitor application as an efficient electrode material," *Vacuum*, vol. 181, p. 109646, 2020.

https://doi.org/10.1016/j.vacuum.2020.109646.

[23] C.-C. Hu and H. Teng, "Structural features of p-type semiconducting NiO as a co-catalyst for photocatalytic water splitting," *Journal of Catalysis*, vol. 272, no. 1, p. 1–8, 2010.

https://doi.org/10.1016/j.jcat.2010.03.020.

[24] Y. M. Putri *et al.*, "Effect of applied potentials and electrolyte concentrations on porous nickel oxide growth by anodization methods for non-enzymatic urea detection," *Microchemical Journal*, p. 114880, 2025.

https://doi.org/10.1016/j.microc.2025.114880.

[25] T. Lkhagvaa, Z. U. Rehman, and D. Choi, "Post-anodization methods for improved anticorrosion properties: A review," *Journal of Coatings Technology Research*, vol. 18, no. 1, p. 1–17, 2021.

https://doi.org/10.1007/s11998-020-00367-8.

[26] J. Joy, J. Mathew, and S. C. George, "Nanomaterials for photoelectrochemical water splitting–review," *International Journal of hydrogen energy*, vol. 43, no. 10, p. 4804–4817, 2018.

https://doi.org/10.1016/j.ijhydene.2018.01.099.

[27] H. Q. Faris and R. Aljarrah, "Employ ZnO/NiO Nanocomposites as Catalyst for Photo Degradation of Methylene Orange Dye in Water," *Journal of Nano Materials Impact*, vol. 1, no. 2, p. 10–16, 2025.

https://doi.org/10.71109/nmi.2025.1.2.11.

[28] A. Ahmed, T. Ali, M. Naseem Siddique, A. Ahmad, and P. Tripathi, "Enhanced room temperature ferromagnetism in Ni doped SnO_2 nanoparticles: A comprehensive study," *Journal of Applied Physics*, vol. 122, no. 8, 2017.

https://doi.org/10.1063/1.4999830.

[29] N. P. Golhar, "Synthesis and structural characterizations of ZnO@NiO nanocomposite," *International Journal on Science*, vol. 15, no. 1, 2024.

[30] Y. Mai, J. Tu, X. Xia, C. Gu, and X. Wang, "Co-doped NiO nanoflake arrays toward superior anode materials for lithium ion batteries," *Journal of Power Sources*, vol. 196, no. 15, p. 6388–6393, 2011.

https://doi.org/10.1016/j.jpowsour.2011.03.089.

[31] X. Tao *et al.*, "Preparation of Co doped NiO thin films with excellent switching time and coloring efficiency through sol-gel spin coating," *Thin Solid Films*, vol. 779, p. 139935, 2023.

https://doi.org/10.1016/j.tsf.2023.139935.

[32] S. Chakrabarty and K. Chatterjee, "Synthesis and Optical Manifestation of NiO - Silica Nanocomposite," *International Scholarly Research Notices*, vol. 2011, no. 1, p. 719027, 2011.

https://doi.org/10.5402/2011/719027.

[33] M. N. Siddique, A. Ahmed, T. Ali, and P. Tripathi, "Investigation of optical properties of nickel oxide nanostructures using photoluminescence and diffuse reflectance spectroscopy," in *AIP conference proceedings*, 2018, vol. 1953, no. 1, p. 030027: AIP Publishing LLC.

https://doi.org/10.1063/1.5032362.

[34] M. Deshpande, K. N. Patel, V. P. Gujarati, K. Patel, and S. Chaki, "Structural, thermal and optical properties of nickel oxide (NiO) nanoparticles synthesized by chemical precipitation method," *Advanced Materials Research*, vol. 1141, p. 65–71, 2016.

https://doi.org/10.4028/www.scientific.net/AMR.1141.65.

[35] M. M. Khan *et al.*, "Band gap engineered TiO_2 nanoparticles for visible light induced photoelectrochemical and photocatalytic studies," *Journal of Materials Chemistry A*, vol. 2, no. 3, p. 637–644, 2014.

https://doi.org/10.1039/C3TA14052K.

[36] C. Wu *et al.*, "Mo, Co co-doped NiS bulks supported on Ni foam as an efficient electrocatalyst for overall water splitting in alkaline media," *Sustainable Energy and Fuels*, vol. 4, no. 4, p. 1654–1664, 2020.

https://doi.org/10.1039/C9SE00822E.

[37] B. J. Rani, G. Ravi, R. Yuvakkumar, S. Ravichandran, F. Ameen, and A. Al-Sabri, "Efficient, highly stable Zn-doped NiO nanocluster electrocatalysts for electrochemical water splitting applications," *Journal of*

Downloaded from https://nanomatimp.uomustansiriyah.edu.iq/

Copyright © 2026. This work licensed under a Creative Commons Attribution Noncommercial 4.0 International License.

Sol-Gel Science and Technology, vol. 89, no. 2, p. 500–510, 2019.

https://doi.org/10.1007/s10971-018-4886-5.

[38] G. Wang *et al.*, "Free-standing nickel oxide nanoflake arrays: synthesis and application for highly sensitive non-enzymatic glucose sensors," *Nanoscale*, vol. 4, no. 10, p. 3123–3127, 2012.

https://doi.org/10.1039/c2nr30302g.

[39] J. Kibsgaard and T. F. Jaramillo, "Molybdenum phosphosulfide: an active, acid - stable, earth - abundant catalyst for the hydrogen evolution reaction," *Angewandte Chemie International Edition*, vol. 53, no. 52, p. 14433 – 14437, 2014.

https://doi.org/10.1002/anie.201408222.

[40] P. Jongnavakit, P. Amornpitoksuk, S. Suwanboon, and T. Ratana, "Surface and photocatalytic properties of ZnO thin film prepared by sol–gel method," *Thin Solid Films*, vol. 520, no. 17, p. 5561–5567, 2012.

https://doi.org/10.1016/j.tsf.2012.04.050.

[41] B.-S. Wang, R.-Y. Li, Z.-Y. Zhang, X.-L. Wu, G.-A. Cheng, and R.-T. Zheng, "An overlapping ZnO nanowire photoanode for photoelectrochemical water splitting," *Catalysis Today*, vol. 321, p. 100–106, 2019.

https://doi.org/10.1016/j.cattod.2018.02.028.

[42] F. Ajala *et al.*, "The influence of Al doping on the photocatalytic activity of nanostructured ZnO: The role of adsorbed water," *Applied Surface Science*, vol. 445, p. 376–382, 2018.

https://doi.org/10.1016/j.apsusc.2018.03.141.

[43] M. R. Islam, M. Rahman, S. Farhad, and J. Podder, "Structural, optical and photocatalysis properties of sol–gel deposited Al-doped ZnO thin films," *Surfaces and Interfaces*, vol. 16, p. 120–126, 2019.

https://doi.org/10.1016/j.surfin.2019.05.007.

[44] A. Qayoom Mugheri, U. Aftab, M. Ishaq Abro, S. R. Chaudhry, L. Amaral, and Z. H. Ibupoto, "Co_3O_4/NiO bifunctional electrocatalyst for water splitting," *Electrochimica Acta*, vol. 306, p. 9–17, 2019.

https://doi.org/10.1016/j.electacta.2019.03.092.

[45] F. Zhao and H. Ma, "Application of Co_3O_4 in photoelectrocatalytic treatment of wastewater polluted with organic compounds: a review," *Crystals*, vol. 13, no. 4, p. 634, 2023.

https://doi.org/10.3390/cryst13040634.

[46] H. Bai *et al.*, "Fabrication of $BiVO_4$-Ni/Co_3O_4 photoanode for enhanced photoelectrochemical water splitting," *Applied Surface Science*, vol. 538, p. 148150, 2021.

https://doi.org/10.1016/j.apsusc.2020.148150.

[47] S. A. Shabbir *et al.*, "Bifunctional Co_3O_4/g-C_3N_4 hetrostructures for photoelectrochemical water splitting," *ACS Omega*, vol. 9, no. 19, p. 21450–21458, 2024.

https://doi.org/10.1021/acsomega.4c01677.

Downloaded from https://nanomatimp.uomustansiriyah.edu.iq/

Copyright © 2026. This work licensed under a Creative Commons Attribution Noncommercial 4.0 International License.